

## PHOTODEGRADATION OF CONTAMINANTS AND ANTIBACTERIAL ACTIVITY ENHANCED BY AgCl NANOPARTICLES ON N, S, Co-DOPED TiO<sub>2</sub> THIN FILMS

L. SIKONG<sup>a,b\*</sup>, B. NOOPHUM<sup>a,b</sup>, K. KOOPTARNOND<sup>a,b</sup>

<sup>a</sup>Department of Mining and Materials Engineering, Faculty of Engineering, Prince of Songkla University, Hat Yai, Songkhla 90112, Thailand

<sup>b</sup>The Materials Engineering Research Center (MERC), Prince of Songkla University, Hat Yai, Songkhla, Thailand 90110

With a view to water treatments ensuring access to potable water, AgCl nanoparticles were deposited on N, S co-doped TiO<sub>2</sub> films immobilized on glass fibers. Their effects on the photodegradation of bisphenol A, 2,4-DCP and antibacterial activity against *E.coli* and *S.aureus* were evaluated. The pure TiO<sub>2</sub> and N, S co-doped TiO<sub>2</sub> films (5NST) coated on glass fibers were prepared by sol-gel and dip coating methods, and calcined at 300°C holding for 2 h. The AgCl nanoparticles were then deposited on the films by a chemical method, and calcined at 400°C for 2 h. The synthesized coatings were characterized by XRD, FTIR, UV-vis DRS, SEM, EDX and XPS. The AgCl nanoparticles on N, S co-doped TiO<sub>2</sub> (A5NST) films had about 40-50 nm crystallite size, and the thickness was about 250-500 nm. The A5NST exhibited higher photocatalytic and antibacterial activities than the 5NST and the pure TiO<sub>2</sub>, because the AgCl nanoparticles reduced the band gap energy and thereby responded to visible light of TiO<sub>2</sub> film. In the best experimental cases, the A5NST coatings eradicated the water contaminants almost completely within 13 h and antibacterial activity of *E. coli* and *S.aureus* in about 40 min and 50 min respectively. The A5NST film can also inhibit bacteria in some degree without any light exposure due to the effect of AgCl on disinfection.

(Received February 21, 2015; Accepted April 29, 2015)

**Keywords:** AgCl nanoparticles, TiO<sub>2</sub> photocatalyst, Photodegradation of bisphenol A and 2,4-DCP. Disinfection of negative and positive gram bacteria

### 1. Introduction

Phenolic compounds are highly toxic affecting human health and aquatic ecosystems. Environmental emissions occur in the wastewaters from petroleum refineries, coal industries, epoxy resin or plastic manufacturing plants, and from making dyestuffs or pharmaceutical and medical supplies [1-3]. Phenols are detectable in surface water, groundwater, sediments, rainwater, along with drinking water. However, drinking phenol contaminated water may initially damage the kidneys and the liver, and may increase the risk of cancer in the longer run. Ingestion of highly phenol contaminated water can cause death. [4, 5] The World Health Organization (WHO) recommends that the phenol concentration in treated water should be <2µg/l, and <1µg/l in drinking water. The concentrations of certain phenols, namely chlorophenol, and 2,4,6-trichlorophenol, should be <0.1µg/l in drinking water [6, 7]. In Thailand, the drinking water quality regulations require that the concentration of phenols is <1µg/l. In addition, harmful bacteria that increasingly contaminate water supplies affect human health. Diarrhea is a serious illness and often causes deaths when clean drinking water is lacking. The WHO/UNICEF Joint Monitoring Program of Water Supply and Sanitation (JMP) reported that 88 percent of diarrheal deaths were caused by unsafe drinking water [8-12]. In South Africa, in 1998, 4 million cases of diarrhea causing 2.5 million deaths were estimated, according to WHO [13].

---

\*Corresponding author: lek.s@psu.ac.th

The compound  $\text{TiO}_2$  is widely used as a white pigment, but also in the purification and detoxification of environment, specifically of water and air [14, 15]. It is used extensively to degrade harmful organic compounds and bacteria contaminating water. The photocatalytic activity of titanium dioxide has been improved by doping it with metal oxides, metals, or non-metallic materials that reduce the band gap energy. The doping retard the recombination of photo-generated electrons and holes, increases the specific surface area of the photocatalyst, and controlling the structure of the  $\text{TiO}_2$  film. The photocatalytic mechanism is based on reactive hydroxyl radicals ( $\text{HO}\cdot$ ) that are generated under light irradiation [16]. Silver nanoparticles (AgNPs) have shown potential in antibacterial [17-19] and water disinfection applications [20-22]. Recently,  $\text{TiO}_2$  films with deposited AgNPs have exhibited high disinfection performance [23-25].

In this work, the effect of silver chloride nanoparticles on the photocatalytic and antibacterial performances of  $\text{TiO}_2$  composite film in water treatment under UV, fluorescent light and in dark condition were investigated. From our previous study [26], the 5 mol% N, S co-doped  $\text{TiO}_2$  (5NST) films on glass fibers have a high photocatalytic performance, and they were used as substrates for AgCl nanoparticles deposition. AgCl nanoparticles on 5NST film expect to be able to improve the photocatalytic performance on degradation of organic pollutant and bacteria. Since it was found that the the AgCl doped  $\text{TiO}_2$  exhibited an excellent photocatalytic activity under visible light and stable for degrading pollution and bacteria [27-31]. Their photocatalytic efficiencies were determined for the degradation of bisphenolA (BPA), 2,4-dichlorophenol (2,4-DCP), and for the antimicrobial properties against *Escherichia coli* (*E.coli*) and *Staphylococcus aureus* (*S.aureus*) under either UV or fluorescent light irradiation or dark condition.

## 2. Experimental

### 2.1 Films Preparation

The films of doped or pure  $\text{TiO}_2$  were prepared via a sol-gel process to coat E-type glass fibers. The pure  $\text{TiO}_2$  (PT) films were prepared by adding 10 ml titanium (IV) isopropoxide (TTIP, 99.95%, Fluka Sigma-Aldrich) drop-wise under vigorous stirring to dissolve it into 150 ml ethanol (99.9%, Merck Germany). The suspension/solution was further stirred for 60 min, and adjusting to pH~3.5 with conc. HCl (36.5-38.0%, Baker Analyzed) caused the formation of  $\text{TiO}_2$  sol. The glass fibers were cleaned and their surfaces modified by soaking in 1 M NaOH solution for 60 min, removing from the solution and washing repeatedly with distilled water, and then drying at 80 °C for 24 h. These treated glass fibers were dipped into the  $\text{TiO}_2$  sol to film coat them, dried in air and calcined. For calcination the heating rate was 10°C/min to 300°C, at which the samples were held for 2 h. For the 5NST films, 5mol% thiourea ((CS (NH<sub>2</sub>)<sub>2</sub>, 98.0%, Ajax Finechem) was used as the source of nitrogen, and this was added with sulfur into the as-prepared  $\text{TiO}_2$  sol, stirred at room temperature for 60 min, and adjusted to pH 3.5 in order to form the coating sol [26]. The 5NST films were dip coated onto glass fibers. These 5NST coated glass fibers were utilized as the substrates for depositing AgCl nanoparticles (A5NST). The concentration of AgCl was fixed at 0.01 mol% obtained from the best result of preliminary study that AgCl dosage varied from 0.01 to 0.3 mol%. Silver nitrate (AgNO<sub>3</sub>, 99.0%, Bosch) for the 0.01 molar ratio was added into distilled water, and then ammonium hydroxide (NH<sub>4</sub>OH, 26-28%, J.T. Baker) was added into the silver nitrate solution, so that its color suddenly changed from clear to dark brown and finally changed to clear again. Then 0.7 M sucrose (C<sub>12</sub>H<sub>22</sub>O<sub>11</sub>, 98.0%, Ajax Finechem) was introduced to the clear solution to make a silver nitrate-sucrose solution used for deposition. The as-prepared 5NST film coated glass fibers were soaked in the silver nitrate-sucrose solution holding for 15 min, then dried in air and calcined at 400°C for 2 h; the heating rate was 5°C/min. The excess loosely deposited AgCl particles were removed in an ultrasonic bath, with immersion for 15 min in distilled water. Then, the coated glass fibers were dried at 80°C for 24 h, and kept in a desiccator until testing.

### 2.2 Materials characterization

Surface morphology was investigated by scanning electron microscopy (SEM) and by energy-dispersive x-ray spectroscopy (EDX). The phases of doped and undoped  $\text{TiO}_2$  were

identified by using an x-ray diffractometer (XRD) (Phillips Expert MPD, Cu-K). The infrared spectra were recorded using a Fourier-transform infrared spectrophotometer (FT-IR) (EQUINOX55, Bruker, Germany) in diffuse reflectance mode across 4000–400  $\text{cm}^{-1}$ , with KBr as the blank. The crystallite size was estimated from XRD by using the Scherer equation. The chemical composition of the films was investigated by X-ray photoelectron spectrometer (XPS; AXIS ULTRA<sup>DLD</sup>, Kratos analytical, Manchester, UK). Spectrums were process on software “VISION II” by Kratos analytical, Manchester, UK. The base pressure in the XPS analysis chamber was about  $5 \times 10^{-9}$  torrs. The samples were excited with X-ray hybrid mode 700x300  $\mu\text{m}$  spot area with a monochromatic Al  $K_{\alpha 1,2}$  radiation at 1.4 keV. X-ray anode was run at 15kV, 10 mA and 150 W.

### 2.3 Photocatalytic activity test

The photocatalytic activities of PT and 5NST (calcined at 300°C) and A5NST (calcined at 400°C) were investigated by observing the degradation of bisphenolA (BPA) and of 2,4-dichlorophenol (2,4-DCP) contaminants in water, under either UV or fluorescent illumination. These batch photocatalytic tests were performed by loading 2 g of the coated glass fibers in 50 ml of an aqueous solution, with an initial 10 ppm concentration of BPA or 2,4-DCP. Before activation by illumination, the fiber suspension was kept in a dark chamber for 60 min to equilibrate adsorption to the film coatings. Both ultraviolet (black light) and fluorescent (white light) lamps had a nominal 110 W power rating, and the irradiation times ranged from 0 to 12 h. The distance between a sample and the light source was fixed at 32 cm. The initial and final concentrations of each contaminant, in the experiments with designated irradiation times, were measured by a UV-vis spectrophotometer (GENESYS), and the ratio of final to initial concentration,  $C/C_0$ , was used as a performance indicator in comparisons. The stability of the films coatings on glass fibers was also investigated by repeated activity tests of the same films for several cycles. The films were subjected to photocatalytic-self cleaning between each cycle.

### 2.4 Photocatalytic antibacterial test

The gram-negative bacteria *Escherichia coli* were used for the antibacterial activity testing of the film coated glass fibers. The bacteria were grown aerobically in 4 ml of tryptic soy broth, at 37°C for 24 h. The bacterial solution was then diluted in 0.85% NaCl, and the initial bacterial concentration was set to  $10^5$  colony forming units (CFU)/ml. A bacterial suspension of 50 ml volume was then treated with 2 g of coated glass fibers, under UV or fluorescent 50 W lamp, or without light irradiation, for a designated time. The 0.1 ml sample of the treated suspension was taken and spread onto a Macconkey agar plate. Each plate was incubated at 37°C for 24 h, and the number of viable *E.coli* colonies was counted. The gram-positive bacteria *Staphylococcus aureus* were also used for the antibacterial activity testing. The method and experimental were using similarly the gram-negative bacteria, it was districted in culture media. The Nutrient agar were used for gram-positive bacteria culture.

Another approach to demonstrate disinfection is the inhibition zone method, in which a clear zone (the disinfection or inhibition zone) surrounding the photocatalytic films was observed. The 0.1 ml sample of initial bacterial concentration  $10^5$  CFU/ml was spread evenly onto a Macconkey agar plate for *E.coli* and onto Nutrient agar plate for *S.aureus* and then films coated glass fibers dimension length 20 mm and width 5 mm were placed as spots on these culture plates. After the cultures were incubated at 37°C in a dark chamber overnight, the average clear zone thicknesses around the coated fibers was determined the length of zone inhibition and recorded.

The bacterial cells, after the various photocatalytic treatments of 30 min duration, were observed by SEM imaging. Preparation by fixed with 0.05% of glutaraldehyde in phosphate buffer saline, and dehydrated by alcohol solutions (50%, 70%, 80%, 90% and 100% alcohol) for 30 min in each solution. After dehydrated were dried in a critical-point dryer and characterized by SEM respectively.

### 3. Results and discussion

#### 3.1 Microstructure of as-synthesized films

The XRD patterns of calcined PT, 5NST and A5NST films are shown in Fig.1. Only anatase phase was found in the PT and 5NST films, with major peaks in agreement with the JCPDS file 76-1940 database [32], namely at  $2\theta$  values of  $25.3^\circ$ ,  $37.9^\circ$ ,  $47.6^\circ$  and  $54.6^\circ$ . In the A5NST film, both anatase and AgCl phases were present. The anatase peaks are apparent on the planes (101), (004), (105), (200) and (204) [33, 34], while the AgCl phase is indicated by the planes (111), (200), (220), (311) and (222) [35, 36]. The AgCl phase relates to the peaks at  $2\theta$  values of  $27.8^\circ$ ,  $32.2^\circ$ ,  $46.2^\circ$ ,  $54.9^\circ$  and  $57.5^\circ$ , according to the JCPDS file 31-1238 database [37, 38]. As shown in Table 1, all the samples were nanocrystalline, with 10-11 nm  $\text{TiO}_2$  crystallite sizes estimated by the Scherer equation. The AgCl deposited on 5NST films had about 42 nm crystallite size. There was no observable effect by the nitrogen and sulfur co-dopants, or by AgCl deposition, on the crystallite size of  $\text{TiO}_2$ .

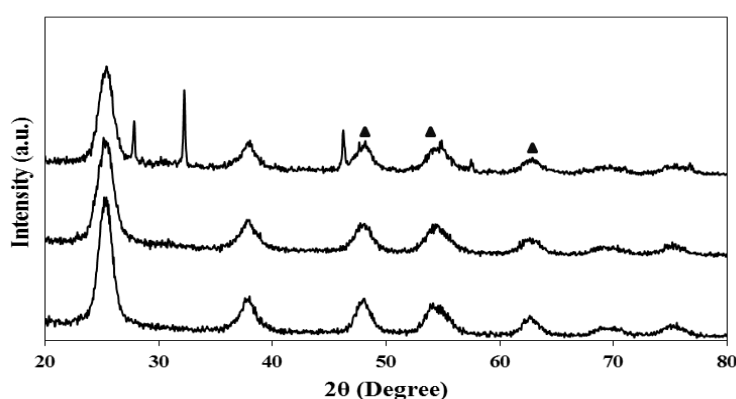


Fig. 1 XRD patterns of the various coatings superposed with vertical shifts: (a) PT calcined at  $300^\circ\text{C}$ , (b) 5NST calcined at  $300^\circ\text{C}$  and (c) A5NST calcined at  $400^\circ\text{C}$ .

Table 1 Crystallite sizes estimated from Scherer equation, phase compositions, and band gap energies of the various coatings on glass fibers, after calcination.

Sample	Anatase crystallite size (nm)	AgCl crystallite size (nm)	Phase (%)	
			Anatase	AgCl
PT calcined at $300^\circ\text{C}$	11.0	-	100	-
5NST calcined at $300^\circ\text{C}$	10.3	-	100	-
A5NST calcined at $400^\circ\text{C}$	10.3	42.0	81.08	18.92

#### 3.2 EDS spectra and morphology of thin films

The EDS spectra of the PT, 5NST and A5NST films in Fig. 2 indicate elements Si, Al, Ca and O, which are common in glass of the fiber substrate. The elements Ti, C and O were found in pure  $\text{TiO}_2$  (PT) film. The Ti, N, S, C and O were found in both 5NST and A5NST samples, while Ag was only found in the A5NST film. The x-ray maps of each element, visualizing their distributions in the films, are also shown in Fig 2. The film coatings with  $\text{TiO}_2$  or doped  $\text{TiO}_2$  provided good coverage of the glass substrate, and the AgCl nanocrystals were also well dispersed on the 5NST films. A trace content of nitrogen was detected in the spectra for 5NST and A5NST, due to its inclusion in the doping.

The morphologies of the thin films are illustrated in Fig.3. The PT film surface is homogenous and smooth (Fig. 3b), while that of 5NST film is rougher (Fig. 3c) due to the agglomeration of  $\text{TiO}_2$  nanocrystals. It is apparent that the deposited AgCl nanocrystals were well dispersed, round in shape, and of a larger size than the  $\text{TiO}_2$  particles (Fig.3d). Cross-sectional

SEM images of the 5NST and A5NST coated glass fibers are shown in Fig.4. The thicknesses of these films were about 100-200 nm for the 5NST, and 250-500 nm for the A5NST. The A5NST film had a rougher surface than the 5NST film.

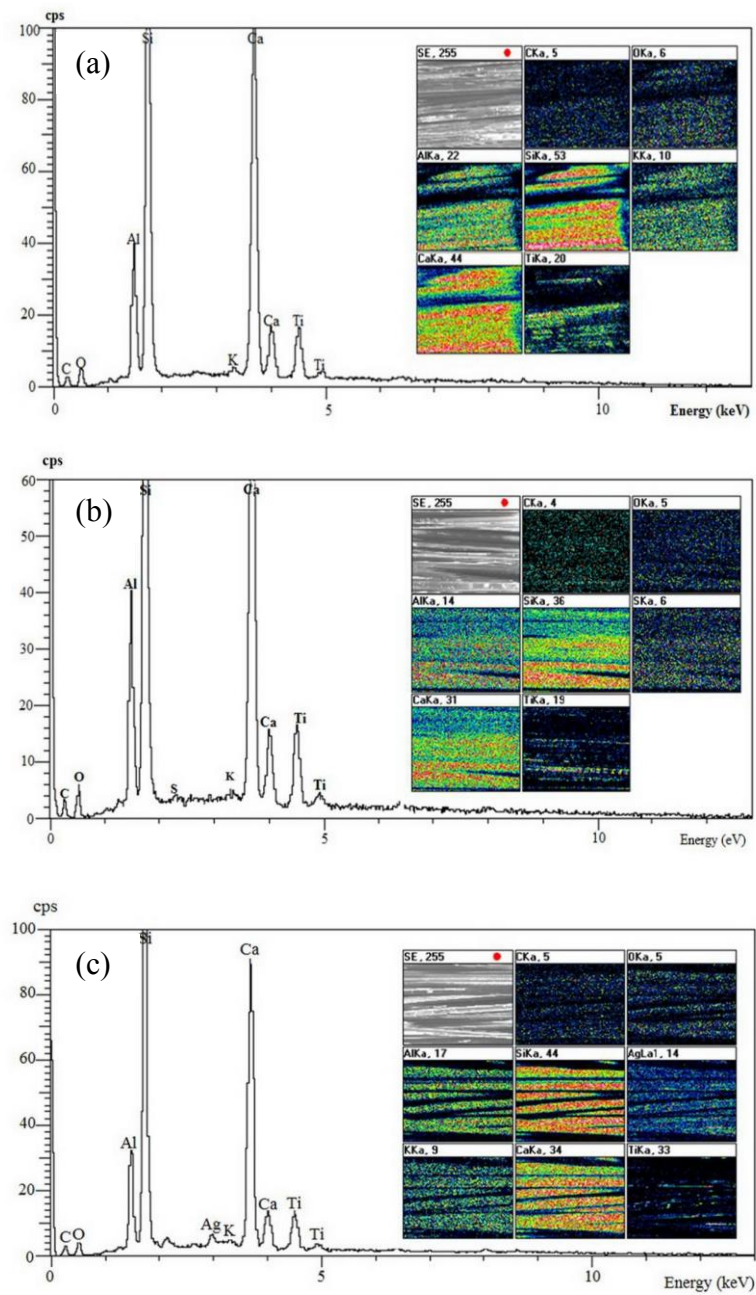


Fig. 2 EDX spectra and X-ray mapping images of coated glass fibers; (a) PT, (b) 5NST calcined at 300 °C, and (c) A5NST calcined at 400 °C.

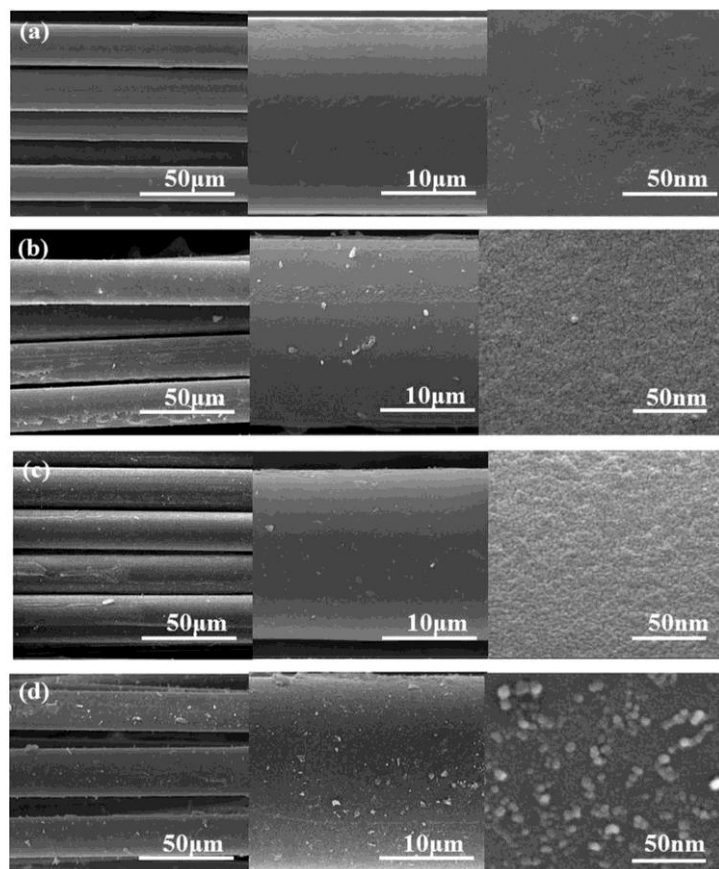


Fig. 3 SEM images of (a) glass fibers, (b) PT calcined at 300 °C, (c) 5NST calcined at 300 °C, and (d) A5NST calcined at 400 °C.

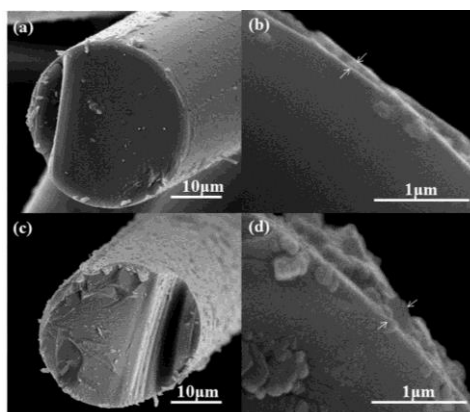


Fig. 4. The cross-sectional SEM images of the 5NST and A5NST coated glass fibers: (a, b) 5NST film calcined at 300 °C, and (c, d) A5NST film calcined at 400 °C.

### 3.3 FTIR analysis

The functional groups and contaminants in the films, introduced by doping with nitrogen and sulfur, and by deposition of silver chloride, were characterized by the FTIR technique. Fig. 5 shows the FTIR spectra of the coatings for wave numbers from 4000 to 400  $\text{cm}^{-1}$ . For  $\text{TiO}_2$ , the band at 3400-3300  $\text{cm}^{-1}$  [39] is assigned to the stretching of hydroxyl groups (Ti-OH); at 1600-1400  $\text{cm}^{-1}$  [40, 41] there is bending of hydroxyl groups; and at 600  $\text{cm}^{-1}$  Ti-O bending [42]. These broad bands from the Ti-O in the 5NST and the A5NST samples are shifted by nitrogen and sulfur

doped into the  $\text{TiO}_2$  lattice, and by the deposited  $\text{AgCl}$ . For the 5NST samples, the band at  $1440\text{ cm}^{-1}$  is assigned to the vibrations of N-H bonds; the band at  $1060\text{ cm}^{-1}$  is from the Ti-O-N interaction; and at  $1030\text{ cm}^{-1}$  is the Ti-O-S interaction [43, 44]. These interactions were also found in the A5NST but not in the pure  $\text{TiO}_2$ . It is noted that the sulfur ions co-ordinate  $\text{Ti}^{4+}$  to form a Ti-O-S bond, and the presence of interstitial nitrogen was demonstrated by Ti-O-N in the doped  $\text{TiO}_2$  samples, as will be later confirmed also by the XPS analysis. The rather narrow bands at  $2900\text{ cm}^{-1}$  and  $2800\text{ cm}^{-1}$  can be assigned to C-H groups.

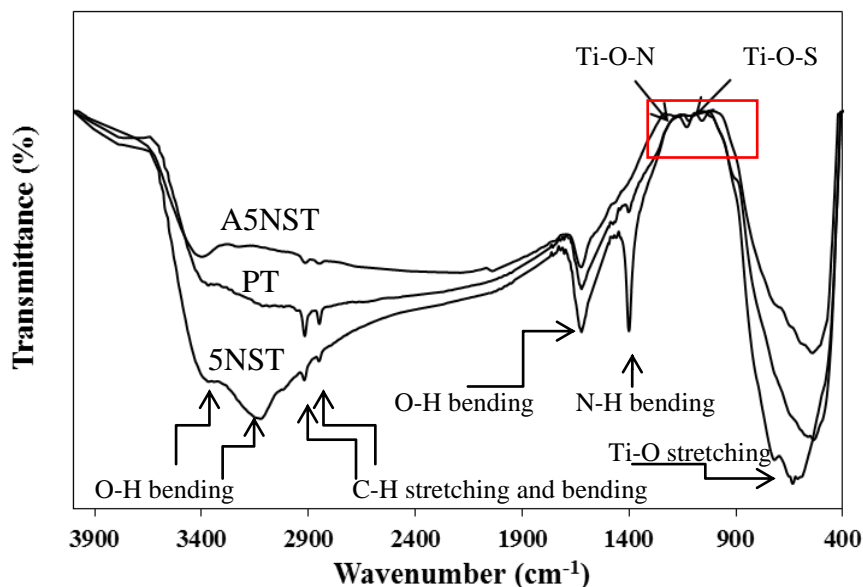


Fig. 5 FTIR spectra of PT calcined at  $300\text{ }^\circ\text{C}$ , 5NST calcined at  $300\text{ }^\circ\text{C}$ , and A5NST calcined at  $400\text{ }^\circ\text{C}$ .

### 3.4 XPS analysis

The effects of nitrogen and sulfur, incorporated into the  $\text{TiO}_2$  films, on the chemical states of N atoms or S atoms, were evaluated by XPS. The spectra of PT and 5NST are shown in Fig. 6. The Ti, O, C, N and S elements are detected, and the binding energies of Ti 2p, O 1s, C 1s, N 1s and S 2p are around 458, 531, 284, 400 and 168 eV, respectively. Magnified regions of the spectra for Ti 2p, O 1s, N 1s, S 2p and C 1s are shown in Fig. 7. As shown in Fig. 7(a), a strong peak at 458.3 eV is attributed to the O-Ti-O linkage, as is also the peak of O 1s at 529.5 eV in Fig. 7(b). The O 1s peak at 531.9 eV corresponds to hydroxyl groups resulting mainly from chemisorbed water. The N 1s spectra of the 5NST film had two convolution peaks at 400.3 and 401.9 eV, shown in Fig. 7 (c), that are attributed to the interstitial nitrogen atoms into the  $\text{TiO}_2$  lattice [45]. These form Ti-N, Ti-O-N and O-Ti-N linkages [46-48], reducing the band gap energy beneficially for the photocatalytic properties of 5NST films. The two peaks at 168.3 and 168.9 eV of S 2p spectrum shown in Fig. 7 (d) correspond to  $\text{S}^{6+} 2p_{3/2}$  and  $\text{S}^{6+} 2p_{1/2}$ , respectively, suggesting that S is incorporated into the lattice of  $\text{TiO}_2$  through substitution for  $\text{Ti}^{4+}$  [49]. However, according to prior work [50, 51] also Ti-S and Ti-N bonding are observed with thiourea doping of  $\text{TiO}_2$ . Fig. 7 (e) depicts the core level peaks of C 1s located at 284.9, 286.1 and 288.3 eV. The peak at 284.9 eV is attributed to elemental carbon on the  $\text{TiO}_2$  surface, while those at 286.1 and 288.3 eV are consistent with the bond C-O and the double bond C=O, respectively [52]. The mass fractions of elements in 5NST from XPS were Ti 16.85%, O 54.21%, C 26.16%, N 1.90% and S 0.88%.

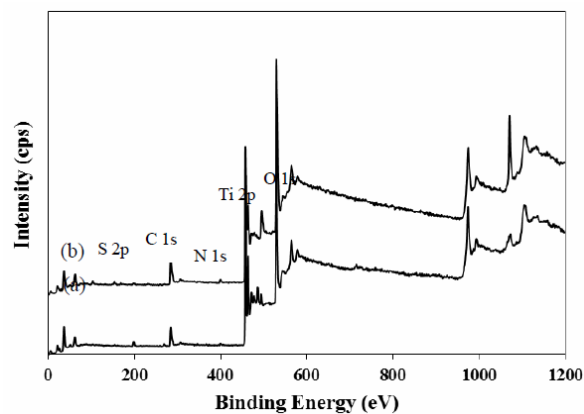


Fig. 6. XPS spectra of (a) PT calcined at 300 °C, and (b) 5NST calcined at 300 °C.

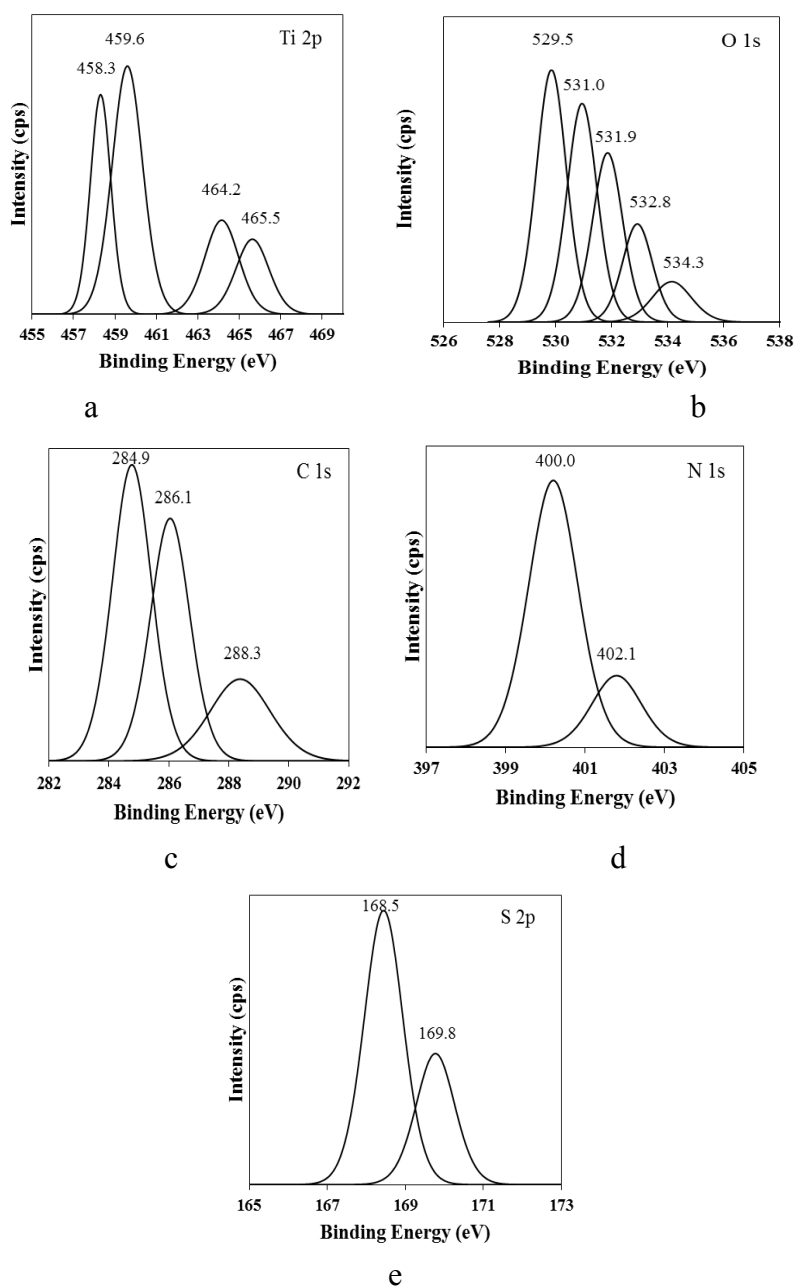


Fig. 7 XPS spectra of 5NST calcined at 400 °C; (a) spectra of Ti 2p, (b) spectra of O 1s, (c) spectra of N 1s, (d) spectra of S 2p, and (e) spectra of C 1s.

### 3.5 Photocatalytic activity

The photocatalytic efficiencies of the coatings were investigated by degrading dissolved BPA and 2,4-DCP, from initial 10 ppm concentrations that exceed the water quality standard 100 folds. The black light and fluorescent lamps providing UV or fluorescent light irradiation had nominal 110 W power. Figs. 8 and 9 show the rates of disappearance of BPA and 2,4-DCP in water, during photocatalytic treatments. An initial 1 hour in darkness was included in all treatments to allow for adsorption equilibrium, and it is seen that the amounts adsorbed were low in all cases. The photocatalytic activities of doped TiO<sub>2</sub> films were higher than with pure TiO<sub>2</sub>. In Fig.8, the A5NST film shows superior degradation of BPA, and it almost completely (99.78%) eradicated BPA with 13 hours of UV irradiation. The 5NST and PT films removed about 80 and 50% of BPA, respectively. In terms of degradation rates, the A5NST was about 0.43 h<sup>-1</sup> better than those of 5NST about 0.14 h<sup>-1</sup> and undoped TiO<sub>2</sub> (PT) about 0.06 h<sup>-1</sup>. While the results of photodegradation of these films under fluorescence irradiation have the same trend (Table 2). The reduced band gap energy of A5NST was mainly caused by the AgCl deposited on the 5NST film, and this reduction facilitates the photocatalytic reactions generated by photo-induced electrons/holes. In addition, the AgCl nanoparticles also act as trapping sites of photo-generated electrons, retarding the recombination of electrons/holes and allowing more time for the photocatalytic reactions to proceed. The BPA photodegradation results under fluorescent and UV irradiation are quite similar, as seen in Fig. 8. However, the PT film exhibited less activity with fluorescent than with UV light, since its 3.20 eV band gap energy requires the more energetic photons of UV light. The work of Katsumata and coworkers [53] deliberate the BPA degradation pathway and its end products. Their results exhibited 93 wt% CO<sub>2</sub> in the products generated from BPA with an initial concentration of 10 mg L<sup>-1</sup> (10 ppm), at 36 h UV irradiation in the presence of 4×10<sup>-3</sup> mol L<sup>-1</sup> H<sub>2</sub>O<sub>2</sub> and 4×10<sup>-4</sup> mol L<sup>-1</sup> Fe(II).

The photocatalytic degradation of 2,4-DCP is shown in Fig.9 and the degradation rates of A5NST, 5NST and PT are summarized in Table 2. It is found that the degradation rate constant of A5NST, 5NST and PT films were about 0.27, 0.16 and 0.09 h<sup>-1</sup>, respectively. Particularly under fluorescent irradiation the doped TiO<sub>2</sub> coatings surpass the undoped coating, and this can be explained by the band gap energies as was done earlier.

The stability of the film coatings on glass fibers was assessed by repeated photocatalytic testing, with results shown in Fig. 10. It is apparent that the efficiency of degrading BPA dropped slightly as the A5NST coatings were re-used for three cycles under fluorescent irradiation, but then remained approximately constantly in further treatment cycles. In contrast, the efficiency remained constant throughout all cycles under UV irradiation. Similarly, the photocatalytic degradation rate of 2,4 DCP by A5NST dropped slightly after 2-3 cycles and then stabilized. These results indicate that TiO<sub>2</sub> films coated on glass fibers possess high stability and can be repeatedly used in batch purification of water, with photocatalytic self-cleaning between the cycles.

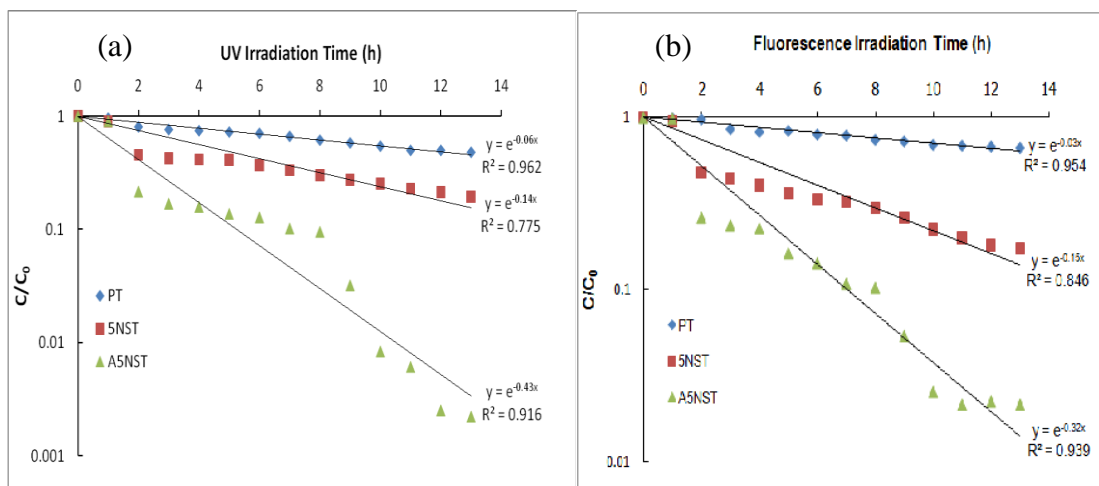


Fig. 8 The photocatalytic degradation of 10 ppm BPA solution under (a) UV and (b) fluorescent 110 W lamps, over 12 h of exposure.

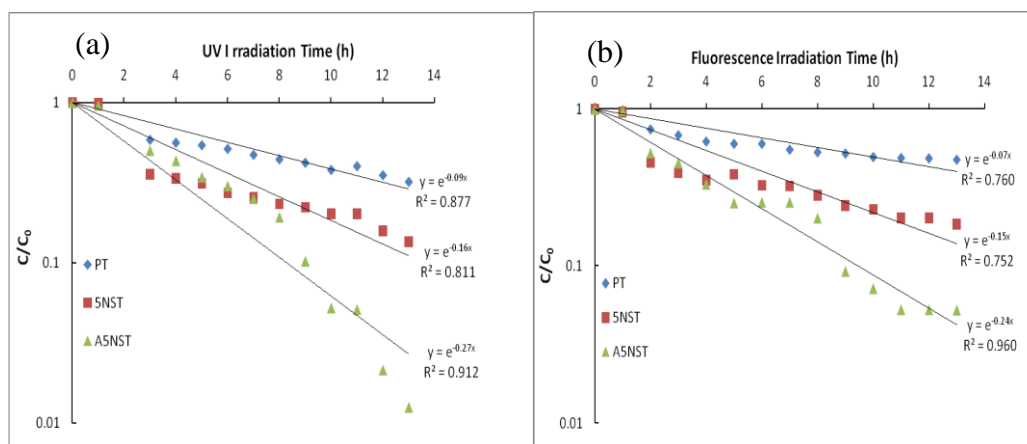


Fig. 9 The photocatalytic degradation of 10 ppm 2,4 DCP solution under (a) UV and (b) fluorescent 110 W lamp, over 12 h of exposure.

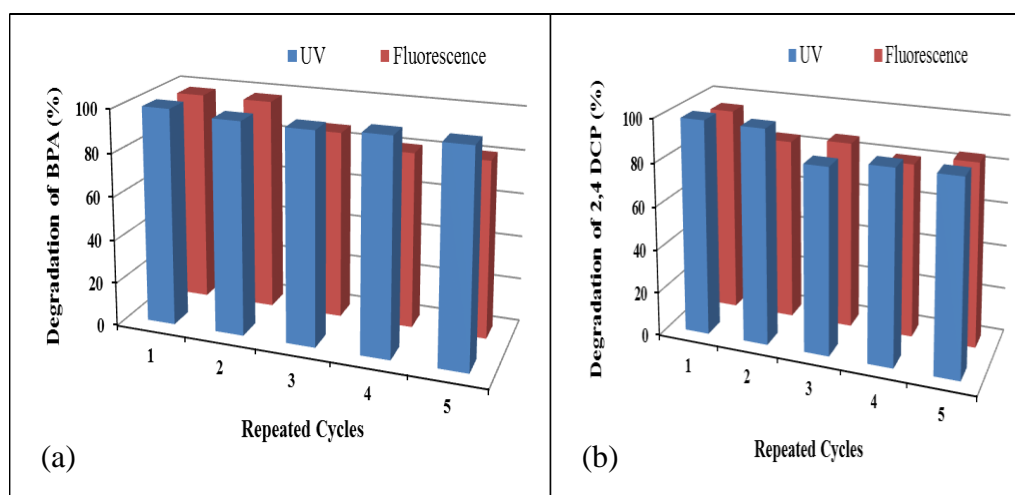


Fig. 10 Photocatalytic batch tests with A5NST were repeated for multiple cycles. The degradation of (a) BPA, and (b) 2,4-DCP, with exposure to UV or fluorescent light for 13 h.

Table 2. The photodegradation rate constant of BPA and 2,4-DCP by the various coatings.

Type of coating	Degradation rate constant, $k$ ( $\text{h}^{-1}$ ) during 13 h under 110 W light			
	BPA		2,4-DCP	
	UV	Fluorescence	UV	Fluorescence
PT calcined at 300°C	0.06	0.03	0.09	0.07
5NST calcined at 300°C	0.14	0.15	0.16	0.15
A5NST calcined at 400°C	0.43	0.32	0.27	0.24

### 3.6 Antibacterial activity

The disinfection effect of the synthesized films on *E.coli* and *S.aureus* were also investigated under UV and fluorescent irradiation, for various times up to 60 min. The bacteria had an initial  $10^5$  CFU/ml concentration. The gram-negative (*E.coli*) antibacterial performance of the coatings, in Fig. 11, was defined by the reduction in colony counts. It was found that A5NST had an excellent performance in killing bacteria under either UV (rate constant,  $k = 0.1 \text{ min}^{-1}$ ) or fluorescent irradiation ( $k = 0.1 \text{ min}^{-1}$ ). The ranking by antibacterial activity of the films by means of a rate constant,  $k$  was A5NST > 5NST > PT, which agrees with the photocatalytic activities. The A5NST films can kill *E.coli* almost completely within 40 min regardless of irradiation, so the

mechanism cannot depend on photoactivity. The gram-positive (*S.aureus*) antibacterial performance of the coatings in terms of the survival rate of bacteria is shown in Fig.12. It was found that A5NST film exhibits an excellent performance in bactericidal under UV ( $k = 0.1 \text{ min}^{-1}$ ) or fluorescent irradiation ( $k = 0.009 \text{ min}^{-1}$ ). The ranking by antibacterial performance of the films by means of a rate constant,  $k$  was A5NST>5NST>PT. The A5NST films can kill *S.aureus* almost completely within 50 min regardless of irradiation. This suggests that the deposited AgCl nanoparticles enhance the strong antibacterial effect of the A5NST film. Images with bacterial inhibition zones, meaning the clear zones surrounding the coated fibers, are shown in Fig. 13 and Fig. 14. The thickness of the clear zone was determined at ten positions as shown in Fig. 13(e), giving an average of 4.2 mm for *E.coli* testing. The inhibition zone of *S.aureus* shown in Fig. 14(e), giving an average of 3.94 mm. The inhibition zone for *S.aureus* is narrower than that for *E.coli* resulting from the gram-positive bacteria having thick cell walls than gram-negative bacteria [54, 55]. The other coatings without AgCl nanoparticles show very thin zones. Fig. 15 and Fig. 16 show SEM images of the bacteria cells after photocatalytic treatments under UV irradiation for 30 min. It was found that cell walls of the *E.coli* and *S.aureus* treated by the A5NST and 5NST coatings are clearly destroyed. The cell walls and cell membranes were damaged also by contact with PT activated by UV or visible light. It is known that silver ions can penetrate bacterial cells and damage the DNA, and silver nanoparticles are nowadays widely used for disinfection.

### 3.7 Mechanism of AgCl nanoparticles on 5NST photocatalytic film

In addition of this study was taking into the photocatalytic activity of  $\text{TiO}_2$ , and affected of AgCl to modifying the  $\text{TiO}_2$  photocatalytic efficiency. AgCl has been sensitively to photo illumination; it was explicated under UV and visible irradiation for disinfection.

Under UV light illumination, electron-hole pairs are created by AgCl particles. The electron-hole pairs were prevented the recombination, or electron and hole may be separate and finally be trapping as reduced Ag atom ( $\text{Ag}^0$ ), or  $\text{Cl}^0$  atom. In generally, the electrons were captured by  $\text{O}_2$  to form superoxide ions ( $\text{O}_2^{\cdot-}$ ). The superoxide ions using for degrade the dye. However, the metallic silver, Ag atoms had seem illustrate that the trapping of free electron by  $\text{Ag}^+$  ions in the matrix. The remaining holes were diffused into the AgCl matrix to oxidizing  $\text{Cl}^-$  ions to Cl atoms. The hole have been oxidizing the adsorbed  $\text{OH}^-$  at the interface to the strong  $\cdot\text{OH}$  radical for dye or chemical pollution and bacteria disinfection.

Under visible light illumination, Ag nanoparticles were producing electrons and holes, which can be separated by the SPR-induced. The holes were generated be transferred to the AgCl surface, thereby resulting in the oxidation of  $\text{Cl}^-$  ions to  $\text{Cl}^0$  atoms. Then, the electrons have trapped by adsorbed  $\text{O}_2$  to form  $\cdot\text{O}_2^{\cdot-}$  while the holes combination by  $\text{OH}^-$  or  $\text{Cl}^-$  ions to form  $\cdot\text{OH}$  or  $\text{Cl}^0$  radicals. The  $\cdot\text{O}_2^{\cdot-}$ ,  $\cdot\text{OH}$ , and  $\text{Cl}^0$  are improved the photocatalytic activity as strong for the degradation of organic pollutants or bacteria [56-59]. Therefore, while the deposited AgCl contributed to the photo-activation and degradation of contaminant chemicals, it appears to have contributed even more significantly to bacterial disinfection.

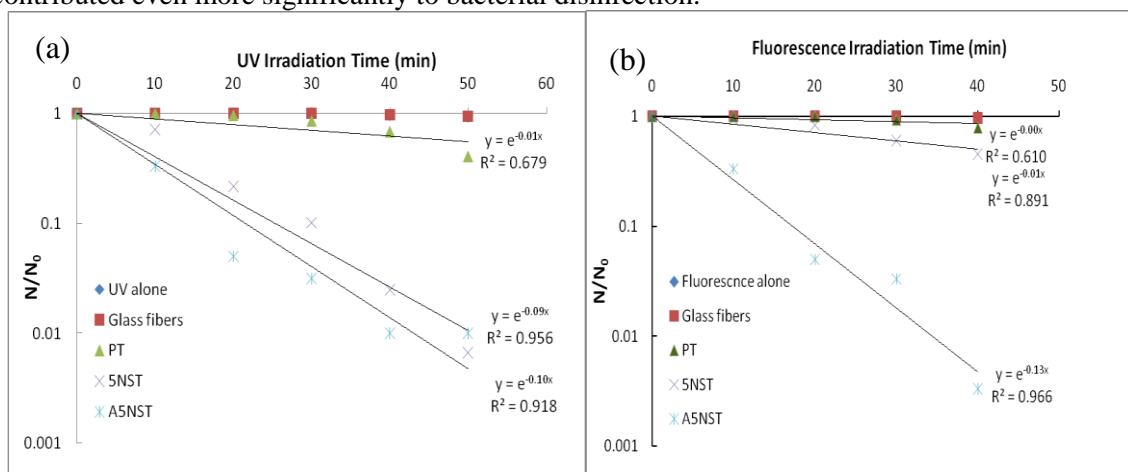


Fig. 11 The antibacterial effects with *E.coli* of the various coatings with exposure to (a) UV and (b) to fluorescent light.

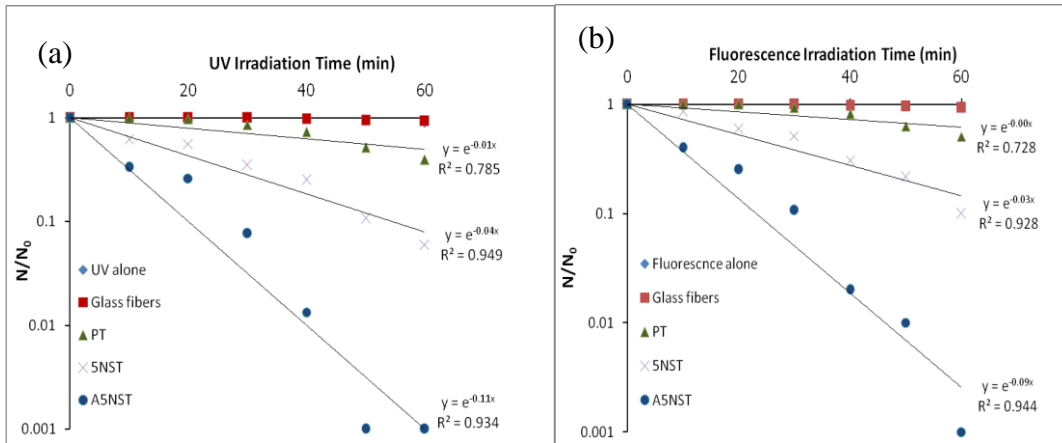


Fig. 12 The antibacterial effects with *S.aureus* of the various coatings with exposure to (a) UV and (b) to fluorescent light.

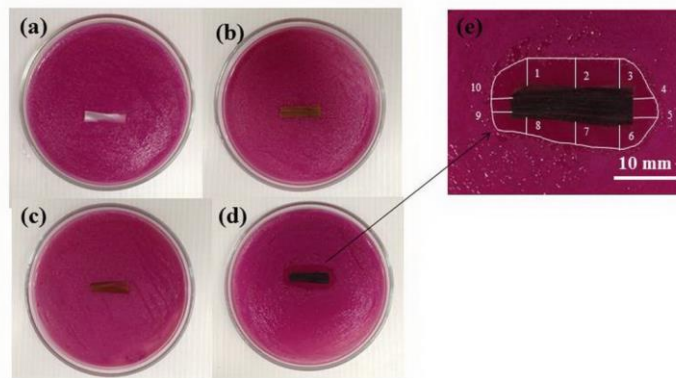


Fig. 13 Bacterial inhibition zones with *E.coli* for (a) Glass fibers, (b) PT, (c) 5NST, and (d) A5NST coated glass fibers. In (e), the measurements to determine the average inhibition zone thickness are schematically shown.

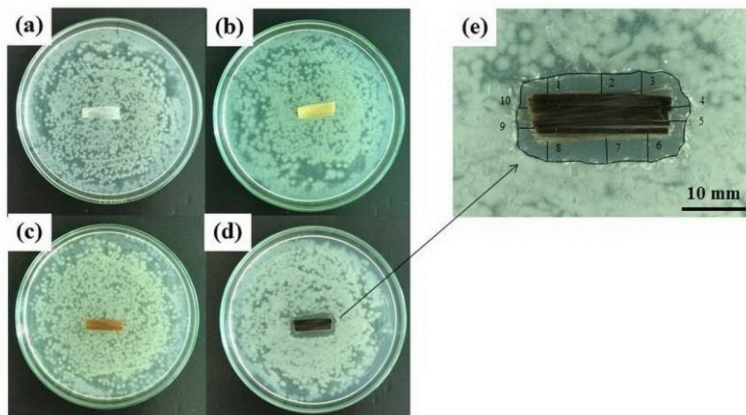
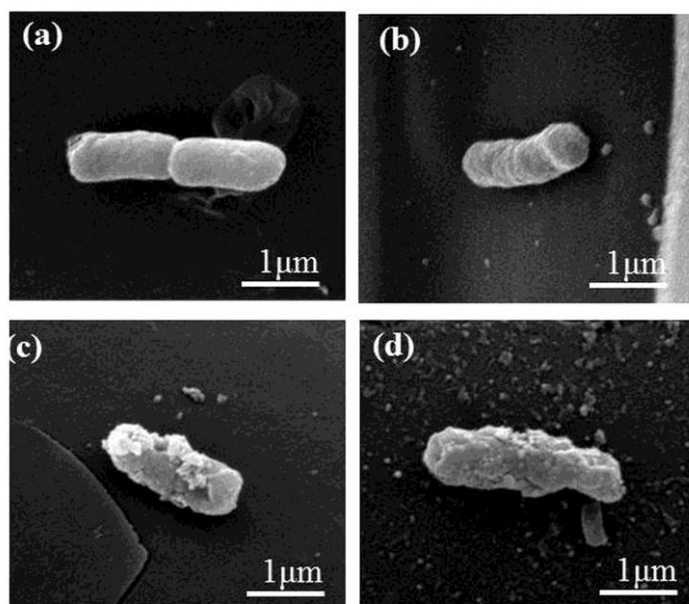
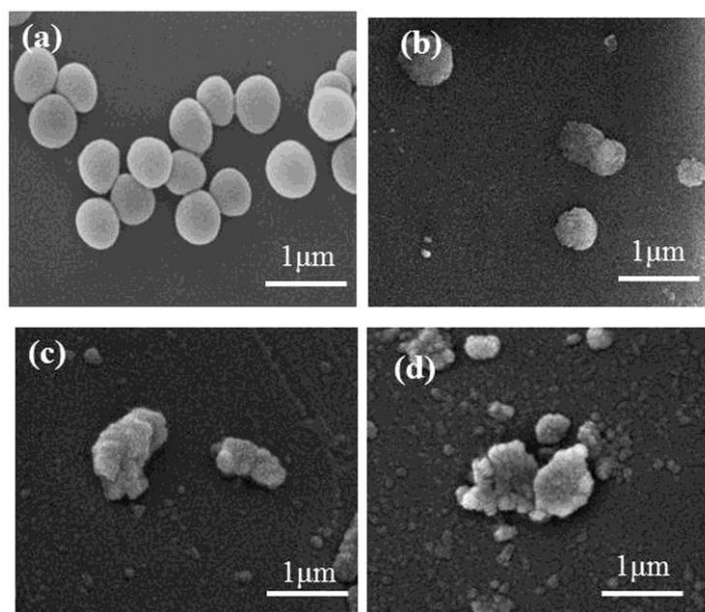


Fig. 14 Bacterial inhibition zones with *S.aureus* for (a) Glass fibers, (b) PT, (c) 5NST, and (d) A5NST coated on glass fibers. In (e), the measurements to determine the average inhibition zone thickness are schematically shown.



*Fig. 15 SEM images of E.coli on the surfaces of (a) Glass fibers, (b) PT, (c) 5NST, and (d) A5NST. These are after a photocatalytic treatment by a 30 min exposure to UV.*



*Fig. 16 SEM images of S.aureus on the surfaces of (a) Glass fibers, (b) PT, (c) 5NST, and (d) A5NST. These was taken after a photocatalytic treatment for 30 min exposure to UV.*

#### 4. Conclusions

Nanoparticles of AgCl were successfully deposited by a chemical process on 5NST thin films on glass fiber substrate. The films were fabricated by sol-gel and dip coating methods, and calcined for 2 h at 400°C that was reached with 5°C /min heating rate. The A5NST coatings had anatase and AgCl phases. The interstitial nitrogen atoms, and the sulfur atoms substituted for titanium atoms in a TiO<sub>2</sub> lattice, shifted the light absorption edge and reduced the band gap energy. The AgCl crystallite size was about 40-50 nm, and the particles were homogenously distributed on the 5NST films. These nanoparticles had a strong effect in shifting the light absorption edge to visible light, and in reducing the band gap energy. Consequently, the A5NST films had strong

photocatalytic activity in degrading BPA and 2,4-DCP under UV or fluorescent lighting. The contaminants were almost completely degraded within 13 h, and antibacterial of *E.coli* and *S.aureus* were similarly treated in less than one hour. In addition, the A5NST film can inhibit bacteria in some degree without any light exposure due to the effect of AgCl on disinfection.

### Acknowledgement

The authors gratefully acknowledge Prince of Songkla University and the Research and Development Office of PSU (RDO) for their financial support. We would like to thank the Materials Engineering Research Center (MERC) and Department of Mining and Materials Engineering, Faculty of Engineering, Prince of Songkla University for their help. Assoc. Prof. Dr. Seppo Karrila, from the Faculty of Science and Technology is also acknowledged for comments and suggestions, as is the copy–editing service of the Research and Development Office of PSU.

### References

- [1] R. C.Wang , C. W. Yu, Ultrason. Sonochem. **20**, 553 (2013).
- [2] H. Friman, A. Schechter, Y. Nitzan and R. Cahan, Int. Biodeter. Biodegr. **84**, 155 (2013).
- [3] Y. Z. Ren, Z. L. Wu, M. Franke, P. Braeutigam, B. Ondruschka, D. J. Comeskey, P. M. King, Ultrason. Sonochem. **20**, 715 (2013).
- [4] Z. Zeng, H. Zou, X. Li, M. Arowo, B. Sun, J. Chen, G. Chu and L. Shao, Chem. Eng. J. **229**, 404 (2013).
- [5] J. Michalwicz, W. Duda , Pol. J. Environ. Stud. **16**, 347 (2007).
- [6] S. Yu, H. J. Yun, Y. H. Kim, J. Yi, Appl. Catal. B-Environ. **144**, 893 (2014).
- [7] World Health Organization. Progress on sanitation and drinking-water 2013. [http://apps.who.int/iris/bitstream/10665/81245/1/9789241505390\\_eng.pdf](http://apps.who.int/iris/bitstream/10665/81245/1/9789241505390_eng.pdf). (Accessed on 5 July 2014).
- [8] World Health Organization. Progress on drinking water and sanitation 2012. [http://whqlibdoc.who.int/publications/2012/9789280646320\\_eng.pdf](http://whqlibdoc.who.int/publications/2012/9789280646320_eng.pdf). (Accessed on 5 July 2014).
- [9] UN Water. Statistics: Graphs & Maps Drinking Water, Sanitation & Hygiene. [http://www.unwater.org/statistics\\_san.html](http://www.unwater.org/statistics_san.html). (Accessed on 15 July 2014).
- [10] UN Water. Statistics: Graphs & Maps Water pollution and environmental degradation. [http://www.unwater.org/statistics\\_pollu.html](http://www.unwater.org/statistics_pollu.html). (Accessed on 15 July 2014).
- [11] Water Pollution and Contaminate. [http://worldsavvy.org/monitor/index.php?option=com\\_content&id=709&Itemid=1195](http://worldsavvy.org/monitor/index.php?option=com_content&id=709&Itemid=1195). (Accessed on 15 July 2014).
- [12] J. Yan, W. Jianping, B. Jing, W. Daoquan, H. Zongding, Biochem. Eng. J. **29**, 227 (2006).
- [13] J. Fawell, M. J. Nieuwenhuisen , Brit. Med. Bull. **68**, 199 (2007).
- [14] K. Laohhasurayotin, S. Pookboonmee, App. Surf. Sci. **282**, 236 (2013).
- [15] M. G. Antoniou, P. A. Nicolaou, J. A. Shoemaker, A. A. Cru, D. D. Dionysiou, Appl. Catal. B-Environ. **91**, 165(2009).
- [16] M. L. Souza, P. Corio, S. Appl. Catal. B-Environ. **136-137**, 325 (2013).
- [17] G. Nangmenyi, X. Li, S. Mehrabi, E. Mintz, J. Economy, Mater. Lett. **65**, 1191(2011).
- [18] C.Y. Chen, C. L. Chiang, Mater. Lett. **62**, 3607(2008).
- [19] J.W. Rhim, L. F. Wang, S. I. Hong, Food Hydrocolloids. **33**, 327(2013).
- [20] A. Dror-Ehre, H. Mamane, T. Belenkova, G. Markovich, A. Adin, J. Colloid Interf. Sci. **339**, 521(2009).
- [21] S. Eduok, B. Martin, R. Villa, A. Nocker, B. Jefferson, F. Coulon, Ecotox. Environ. Safe. **95**, 1(2013).
- [22] D.V. Quang, P. B. Sarawade, S. J. Jeon, S. H. Kims, J. Kim, Y. G. Chai, H. T. Kim, Appl. Surf. Sci. **266**, 280(2013).
- [23] L. He, S. Gao, H. Wu, X. Liao, Q. He, B. Shi, Mater. Sci. Eng-C. **32**, 1050 (2012).

- [24] K.D. Secinti, H. Özalp, A. Attar, M. F. Sargon, *J. Clin. Neurosci.* **18**, 391(2011).
- [25] J. Wang, W. Liu, H. Li, H. Wang, W. Zhou, H. Liu, *Chem. Eng. J.* **228**, 272 (2013).
- [26] B. Noophum, L. Sikong, K. Kooptanond, *Adv. Mater. Res.* **781-784**, 2237(2013).
- [27] M. Long, W. Cai, *Nano Sc.* **6**, 7730 (2014).
- [28] W. Liao, Y. Zhang, M. Zhang, M. Murugananthan, S. Yoshihara, *Che. Eng. J.* **231**, 455 (2013).
- [29] J. Cao, B. Xu, B. Luo, H. Lin, S. Chen, *Appl. Surf. Sci.* **257**, 7083 (2011).
- [30] J. Zhou, Y. Cheng, J. Yu, *J. Photoch. Photobio. A.* **223**, 82 (2011).
- [31] J.F. Guo, B. Ma, A. Yin, K. Fan, W.L. Dai, *J. Hazard. Mater.* **211-212**, 77 (2012).
- [32] W. Mekprasart, W. Pecharapa, *Energy Procedia.* **9**, 509 (2011).
- [33] M. Behpour, V. Atouf, *Appl. Surf. Sci.* **258**, 6595 (2012).
- [34] C. Wen, Y. J. Zhu, T. Kanbara, H. Z. Zhu, C. F. Xiao, *Desalination.* **249**, 621 (2009).
- [35] L. Qi, J. Yu, G. Liu, P. K. Wong, *Catal. Today.* **224**, 193 (2014).
- [36] J.G. McEvoy, W. Cui, Z. Zhang, *Appl.Catal. B-Environ.* **144**, 702 (2014).
- [37] M. Hamadani, A. Reisi-Vanani, A. Majedi, *Appl. Surf. Sci.* **256**, 1837 (2010).
- [38] W. Cui, H. Wang, L. Liu, Y. Liang, J. G. McEvoy, *Appl. Surf. Sci.* **283**, 820 (2013).
- [39] Y. Liang, S. Lin, J. Hu, L. Liu, *J. Mol. Catal. A- Chem.* **383-384**, 231(2014).
- [40] H. Daupor, S. Wongnawa, *Appl. Catal. A-Gen.* **473**, 59 (2014).
- [41] S. Liu, X. Chen, *J. Hazard. Mater.* **152**, 48 (2008).
- [42] J. Senthilnathan, L. Philip, *Chem. Eng. J.* **161**, 83 (2010).
- [43] H. Ming, H. Huang, K. Pan, H. Li, Y. Liu, Z. Kang, *J. Solid State Chem.* **192**, 305 (2012).
- [44] G. Yang, Z. Jiang, H. Shi, M. O. Jones, T. Xiao, P. P. Edwards, Z. Yan, *Appl. Catal. B-Environ.* **96**, 458 (2010).
- [45] P.A.K. Reddy, P.V.L. Reddy, V.M. Sharma, B. Srinivas, V.D.Kumari, M. Subrahmanyam, J. *Water. Res. Prot.* **2**, 235 (2010).
- [46] G. Halasi, I. Ugrai, F. Solymosi, *J. Catal.* **281**, 309 (2011) .
- [47] O. Acik, V. Kiisk, M. Krunks, I. Sildos, A. Junolainen, M. Danilson, A. Mere, V. Mikli, *Appl. Surf. Sci.* **261**, 735(2012).
- [48] J.A. Rengifo-Herrera, E. Mielczarski, J. Mielczarski, N.C. Castillo, J. Kiwi, C. Pulgarin, *Appl. Catal. B-Environ.* **84**, 448 (2008).
- [49] B. Li, X. Cheng, X. Yu, Z. Xing, *Adv. Mater. Sci. Eng.* **2012**, 1 (2012).
- [50] S. Liu, L. Yang, S. Xu, S. Lou, Q. Cai, *Electrochem. Commun.* **11**, 1748 (2009) .
- [51] J.A. Rengifo-Herrera, C. Pulgarin, *Sol. Energy.* **84**, 37 (2010).
- [52] S. Yin, K. Ihara, Y. Aita, M. Komatsu, T. Sato, *J. Photoch. Photobio. A-Chem.* **179**, 105 (2006).
- [53] H. Katsumata, S. Kawabe, S. Kaneco, T. Suzuki, K. Ohta, *J. Photoch. Photobio. A-Chem.* **162**, 297 (2004).
- [54] P. Kongsong, L. Sikong, S. Niyomwas, V. Rachpech, *Sci. World. J.* **2014**, 1 (2014).
- [55] M. Ramani, S. Ponnusamy, C. Muthamizhchelvan, *Mater.Sci. Eng. C.* **32(8)**, 2381(2012).
- [56] H. Chen, L. Xiao, J. Huang, *Mater. Res. Bill.* **57**, 35(2014).
- [57] C. Dong, Z. Yan, J. Kokx, D. B. Chrisey, C.Z.Dinu, *Appl.Surf. Sci.* **258**, 9218 (2012).
- [58] Sh. Sohrabnezhad, M.A. Zanjanchi, M. Razavi, *Spectrochim. Acta. A.* **130**, 129 (2014).
- [59] B. Tian, R.Dong, J.Zhang, S.Bao, F.Yang, J. Zhang, *Appl. Catal. B-Environ.* **158-159**, 76 (2014).